Trends
in Computational and
Applied Mathematics

Rotational Steady Waves in a Low-pressure Region

M. V. FLAMARION

ABSTRACT. Nonlinear steady rotational waves in a low-pressure region are investigated. The problem is formulated in a simplified canonical domain through the use of a conformal mapping, which flattens the free surface. Steady waves are computed numerically using a Newton's method and classified into three types. Besides, our results indicate that there is a region in which steady waves do not exist. The thickness of this region is compared with the one predicted by the weakly nonlinear, weakly dispersive regime.

Keywords: steady waves, rotational waves, shear flow, Euler equations.

1 INTRODUCTION

Waves generated by an external force is of great interest due to the large number of physical applications. For instance, optical fibers, superconductive electronics, elementary-particle physics and water waves [15, 17]. Regarding the last one, we mention, ship waves [2, 18], and waves generated by storms [14]. In water waves, the external force usually models a pressure distribution moving along the free surface. The water is assumed to be inviscid, incompressible, and with constant density.

For an irrotational flow, it is well established that the fundamental parameters used for describing the flow motion generated due to a moving pressure distribution over the water surface is the Froude number

$$F = \frac{U_0}{\sqrt{gh_0}},$$

and the intensity of the applied pressure (δ). Here, U_0 is the velocity of the uniform stream, g is the acceleration of gravity and h_0 is the undisturbed depth of the water channel. The Froude number is called critical when $F = 1$, i.e., when the linear long-wave phase speed is equal to the mean flow speed. In the weakly nonlinear, weakly dispersive regime the forced Korteweg-de Vries (fKdV) arises as a model to study near-resonant flows ($F \approx 1$) with a moving pressure of small amplitude. A detailed study considering the fKdV equation was first done by Wu & Wu [20] and later in [1, 13, 16, 21], and more recently by Grimshaw & Malewoong [11, 12].

Universidade Federal Rural de Pernambuco (UFRPE), UACSA/Unidade Acadêmica do Cabo de Santo Agostinho, BR 101 Sul, 5225, 54503-900, Ponte dos Carvalhos, Cabo de Santo Agostinho, PE, Brazil – E-mail: marcelo.flamarion@ufrpe.br https://orcid.org/0000-0001-5637-7454

In the near-resonant regime, the generated waves have complex patterns which propagates upstream and downstream from where the pressure is applied. These flows may be undesirable since the generated waves can cause problems in applications, such as the erosion of waterway banks and energy loss through wave drag on a ship. This motivates us to study steady solutions in the near-resonant regime. Studying steady waves for the fKdV equation for a localised obstacle, Binder et al. [3] showed that when the forcing is positive ($\delta > 0$), no steady solutions exist for

$$1 - \left(\frac{9\delta}{4\sqrt{2}}\right)^{2/3} < F < 1 + \left(\frac{9\delta}{8\sqrt{2}}\right)^{2/3},$$

and when the forcing is negative ($\delta < 0$), no steady solutions exist for

$$1 - \left(\frac{9|\delta|}{4\sqrt{2}}\right)^{2/3} < F < 1.$$

Regarding the Euler equations, Grimshaw & Malewoong [10] used the full nonlinear model to investigate the stability of stationary fKdV solutions in both the subcritical ($F < 1$) and supercritical ($F > 1$) regimes. It was shown that the main difference between the fKdV model and the Euler model arises when the forcing amplitude is larger. Therefore, for the supercritical case, the fKdV model still predicts an unstable solution with a smooth large amplitude free solitary wave moving away from where the pressure is exerted, but in the Euler model, this large amplitude free solitary wave steepens and may break. The solutions produced by the full nonlinear model may break at early times as we increase δ.

More recently, Flamarion et al. [7] deduced a fKdV in a channel sheared vertically and compared the results with the full nonlinear model, finding qualitatively differences in the flow motion. Although there are many works on rotational waves for the unforced ($P = 0$) problem (the interested reader is referred to Refs ([5, 8, 9] and references therein), as far as we know there are no articles on rotational steady waves when a negative pressure is applied over the free surface.

In this paper we investigate numerically steady wave solutions in a low-pressure region. We find three different types of solutions. Besides, numerical evidences indicate that steady waves do not exist for certain values of the Froude number and the vorticity.

This article is organized as follows. In section 2 we present the mathematical formulation of the problem. The conformal mapping and the numerical methods are presented in section 3. Results are presented in section 4 and the conclusion in section 5.

2   MATHEMATICAL FORMULATION

We consider a two-dimensional incompressible flow of an inviscid fluid with constant density (ρ) in a finite depth channel (h_0), and in the presence of a vertically sheared current with constant vorticity (Ω_0) under the force of gravity (g). By P, we denote a pressure distribution which moves with constant speed (U_0) over the free surface ($\tilde{\zeta}(x,t)$). Under these conditions the velocity field can be written as

$$\nabla\tilde{\phi}(x,y,t) + (-\Omega_0 y, 0),$$

where $\tilde{\phi}(x,y,t)$ is the harmonic component of the velocity field. Using the typical wavelength h_0 as the horizontal and vertical length, $(gh_0)^{1/2}$ as the velocity potential scale, $(h_0/g)^{1/2}$ as the time scale, and $\rho g h_0$ as the pressure scale, we obtain the following dimensionless Euler equations

$$
\begin{aligned}
&\Delta\tilde{\phi} = 0 \ \text{ for } \ -1 < y < \tilde{\zeta}(x,t), \\
&\tilde{\phi}_y = 0 \ \text{ at } \ y = -1, \\
&\tilde{\zeta}_t - \Omega\tilde{\zeta}\tilde{\zeta}_x + \tilde{\phi}_x\tilde{\zeta}_x - \tilde{\phi}_y = 0 \ \text{ at } \ y = \tilde{\zeta}(x,t), \\
&\tilde{\phi}_t + \frac{1}{2}(\tilde{\phi}_x^2 + \tilde{\phi}_y^2) - \Omega\tilde{\zeta}\tilde{\phi}_x + \tilde{\zeta} + \Omega\tilde{\psi} = -P(x+Ft) \ \text{ at } \ y = \tilde{\zeta}(x,t),
\end{aligned}
\tag{2.1}
$$

where $\Omega = \Omega_0 h_0/(gh_0)^{1/2}$ is the dimensionless vorticity and $\tilde{\psi}$ is the harmonic conjugate of $\tilde{\phi}$. It is convenient to consider the equations in the moving framework $x \to x + Ft$. Thus, we define the new functions

$$
\tilde{\zeta}(x-Ft,t) = \bar{\zeta}(x,t), \ \ \tilde{\phi}(x-Ft,y,t) = \bar{\phi}(x,y,t).
$$

Substituting in (2.1) we obtain

$$
\begin{aligned}
&\Delta\bar{\phi} = 0 \ \text{ for } \ -1 < y < \bar{\zeta}(x,t), \\
&\bar{\phi}_y = 0 \ \text{ at } \ y = -1, \\
&\bar{\zeta}_t + (F - \Omega\bar{\zeta} + \bar{\phi}_x)\bar{\zeta}_x - \bar{\phi}_y = 0 \ \text{ at } \ y = \bar{\zeta}(x,t), \\
&\bar{\phi}_t + \frac{1}{2}(\bar{\phi}_x^2 + \bar{\phi}_y^2) + (F - \Omega\bar{\zeta})\bar{\phi}_x + \bar{\zeta} + \Omega\bar{\psi} = -P(x) \ \text{ at } \ y = \bar{\zeta}(x,t).
\end{aligned}
\tag{2.2}
$$

Since we are interested in computing steady waves for (2.2), the free surface and the potential velocity can be written as

$$
\bar{\zeta} = \bar{\zeta}(x) \ \text{ and } \ \bar{\phi} = \bar{\phi}(x,y).
$$

Substituting in (2.2) we obtain the dimensionless Euler equations in the moving framework

$$
\begin{aligned}
&\Delta\bar{\phi} = 0 \ \text{ for } \ -1 < y < \bar{\zeta}(x), \\
&\bar{\phi}_y = 0 \ \text{ at } \ y = -1, \\
&(F - \Omega\bar{\zeta} + \bar{\phi}_x)\bar{\zeta}_x - \bar{\phi}_y = 0 \ \text{ at } \ y = \bar{\zeta}(x), \\
&\frac{1}{2}(\bar{\phi}_x^2 + \bar{\phi}_y^2) + (F - \Omega\bar{\zeta})\bar{\phi}_x + \bar{\zeta} + \Omega\bar{\psi} = -P(x) \ \text{ at } \ y = \bar{\zeta}(x).
\end{aligned}
\tag{2.3}
$$

According to our adimensionalization, $P = 0$ means atmospheric pressure, while positive pressure means a high-pressure region and negative pressure means a low-pressure region. In the next section, we discuss the numerical method to solve (2.3).

3   CONFORMAL MAPPING AND NUMERICAL METHODS

We solve numerically the system (2.3) in the same fashion as done by Dyachenko et al. [6]. First, we construct a conformal mapping f,

$$
f(\xi + i\eta) = x(\xi, \eta) + iy(\xi, \eta),
$$

which flattens the free-surface onto a strip of width D. The conformal mapping satisfyies the boundary conditions

$$y(\xi, 0) = 0 \text{ and } y(\xi, -D) = -1.$$

It is worth noting that the conformal mapping preserves angles. Thus, if we fix the horizontal length of the canonical domain, the vertical width of this strip has to adjust accordingly.
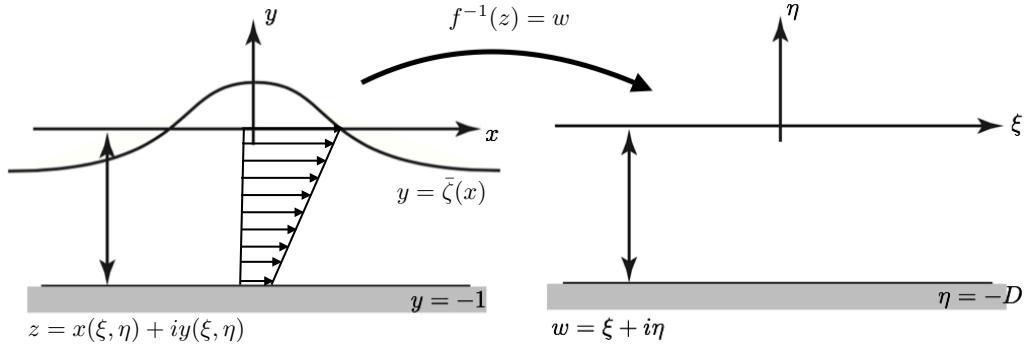
Figure 1: The inverse conformal mapping. The free surface is flattened out in the canonical domain.

Let $\bar{\psi}(x(\xi, \eta), y(\xi, \eta))$ be the harmonic conjugate of $\bar{\phi}(x(\xi, \eta), y(\xi, \eta))$,

$$\phi(\xi, \eta) = \bar{\phi}(x(\xi, \eta), y(\xi, \eta))$$

the potential velocity in the canonical domain and $\Psi(\xi, \eta)$ its harmonic conjugate. Denote by $\Phi(\xi)$ and $\Psi(\xi)$ their traces along $\eta = 0$ and by $X(\xi)$, $Y(\xi)$ the horizontal and vertical free surface coordinates at $\eta = 0$. Substituting these variables in steady Kinematic and Bernoulli condition $(2.3)_{3,4}$ yields when evaluated

$$\begin{aligned}
&\Phi_\xi + F Y_\xi - \Omega Y Y_\xi = 0 \\
&Y + \frac{1}{2J}(\Phi_\xi^2 - \Psi_\xi^2) + \frac{1}{J}(F - \Omega Y)X_\xi \Phi_\xi + \Omega \Psi + P(X) = 0,
\end{aligned} \tag{3.1}$$

where, $J = X_\xi^2 + Y_\xi^2$ is the Jacobian of the conformal mapping evaluated at $\eta = 0$. The horizontal coordinate and the canonical potential velocity satisfy

$$\begin{aligned}
X_\xi &= 1 - \mathscr{C}[Y_\xi], \\
\Phi_\xi &= -\mathscr{C}[\Psi_\xi],
\end{aligned} \tag{3.2}$$

where, $D = 1 + \langle Y \rangle$ is chosen so that that the wavelengths are the same in both the physical and canonical domains and $\mathscr{C} = \mathscr{F}_{k \neq 0}^{-1} i \coth(k_j D) \mathscr{F}_{k \neq 0}$. Fourier modes are given by

$$\mathscr{F}_{k_j}[g(\xi)] = \hat{g}(k_j) = \frac{1}{2L} \int_{-L}^{L} g(\xi) e^{-ik_j \xi} d\xi,$$

$$\mathscr{F}_{k_j}^{-1}[\hat{g}(k_j)](\xi) = g(\xi) = \sum_{j=-\infty}^{\infty} \hat{g}(k_j)e^{ik_j\xi},$$

where $k_j = (\pi/L)j$, $j \in \mathbb{Z}$.

In the next section we discuss a numerical method to solve the problem (3.1)-(3.2).

4   NUMERICAL RESULTS

We consider the computational domain $[-L, L]$, with an uniform grid with N points and step $\Delta\xi = 2L/N$. All derivatives in ξ and the operator $\mathscr{C}$ are performed spectrally [19]. On the grid points ξ_n, $n = 1, 2, ...N$, the steady Bernoulli equation is written as

$$G_n(\boldsymbol{Y}_1, \boldsymbol{Y}_2, ..., \boldsymbol{Y}_N) := \boldsymbol{Y}_n + \frac{1}{2J}(\boldsymbol{\Phi}_{\xi,n}^2 - \boldsymbol{\Psi}_{\xi,n}^2) + \frac{1}{J}(F + \Omega\boldsymbol{Y}_n)\boldsymbol{X}_{\xi,n}\boldsymbol{\Phi}_{\xi,n} + \Omega\boldsymbol{\Psi}_n + P_n.$$

We point out that all unknowns in equations (3.1) can be written in terms of $\boldsymbol{Y}$. The Jacobian for Newton's method is computed using

$$\frac{\partial G_n}{\partial \boldsymbol{Y}_l} = \frac{G_n(\boldsymbol{Y}_1, \boldsymbol{Y}_2, ..., \boldsymbol{Y}_l + \Delta\boldsymbol{Y}, ..., \boldsymbol{Y}_N) - G_n(\boldsymbol{Y}_1, \boldsymbol{Y}_2, ..., \boldsymbol{Y}_l, ..., \boldsymbol{Y}_N)}{\Delta\boldsymbol{Y}}.$$

The stopping criteria

$$\frac{\sum_{j=1}^{N} |G_n(\boldsymbol{Y}_1, \boldsymbol{Y}_2, ..., \boldsymbol{Y}_N)|}{J} < \delta,$$

is used for a give tolerance δ.

The initial guess is $\boldsymbol{Y}_0(\xi) = 0$. The solution can then be continued in the parameters (F, Ω) by using the prior converged solution as the initial guess to a new solution. The pressure is modelled by

$$P(x) = -\varepsilon\exp\left(-x^2/w\right),$$

where ε is the amplitude of the pressure and w its width. This numerical method is a particular case of the one introduced in [7]. The authors tested the sensitivity of the scheme with respect to N and ξ and showed that the solution is accurately captured by different discretizations. Therefore, in all the following simulations, unless mentioned otherwise we consider the following parameters $L = 50$, $N = 1024$, $\delta = 10^{-12}$, $\varepsilon = 0.1$ and $w = 10$.

4.1   Rotational steady waves

Our numerical method is able to capture three types of waves in the plane $\Omega \times F$. Depression solitary waves above where the pressure is applied, non-physical waves and steady waves with permanent tails were found. This type of waves satisfy the requirements of solitary waves except that it has an exponentially small oscillatory field along its sides. In analogy with having very small lateral wings, Boyd [4] defines this wave as a "nanopteron".
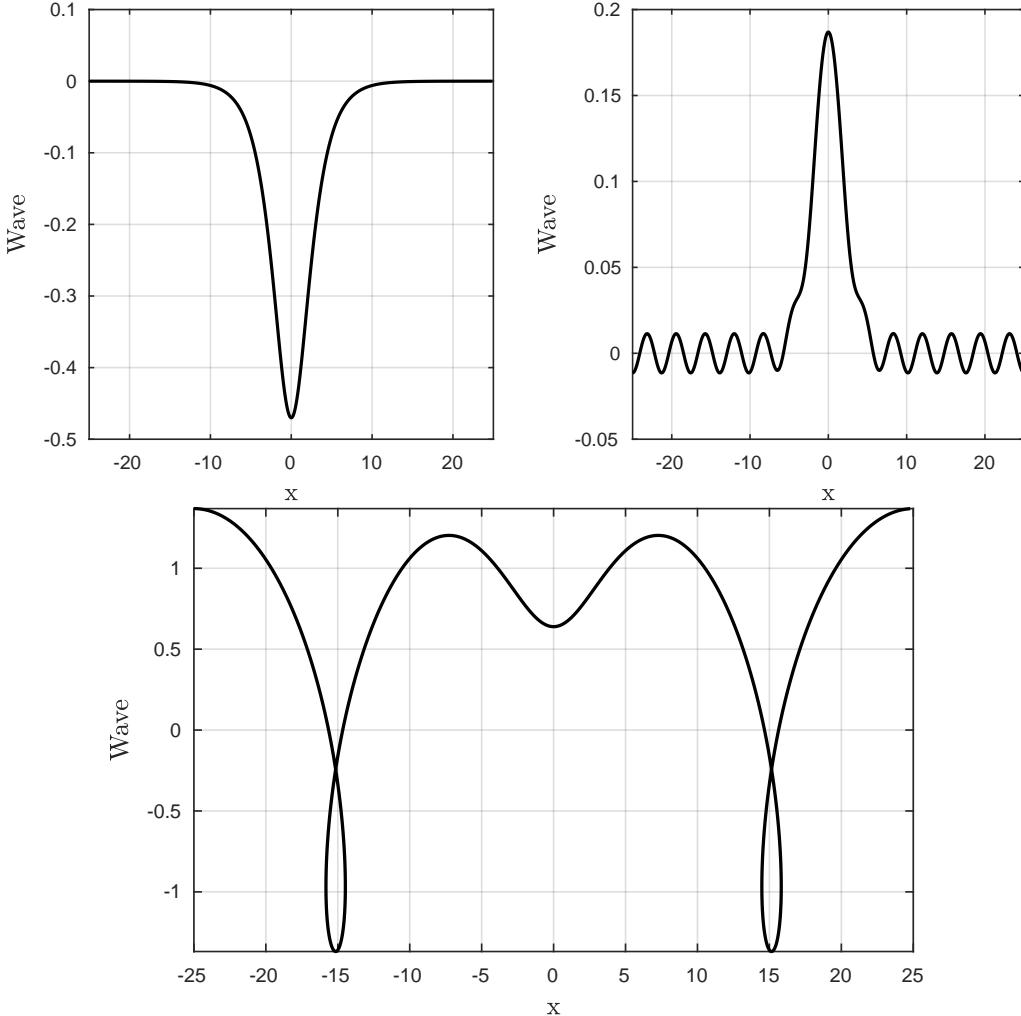
Figure 2: Top (left): typical depression steady solitary wave for $F = 1.3$ and $\Omega = -0.4$. Top (right): typical nanopteron steady solution for $F = 0.9$ and $\Omega = -0.5$. Bottom: non-physical solution for $F = 1.2$ and $\Omega = -0.4$.

Figure 2 displays three typical steady wave solutions of (2.3). It is important to point out that for a given pair (Ω, F), it is not always possible to find a physical steady wave. However, the Newton's method always gives us a solution for every pair (Ω, F).

In the time-dependent problem, the main effect of the vorticity in the generation of waves is that it steepens the waves and the increasing of the wave amplitude indicates that for some value of Ω the generated wave may break [7]. In our experiments, we notice that the wave amplitude increases as Ω decreases until it reaches a certain threshold. Once we cross this threshold the computed solutions are no longer physical solutions. In fact, we can always adjust the parameter

Ω to have sharp crested steady wave solutions. Figure 3 depicts a sharp depression solitary steady wave computed for $F = 1.2$ and $\Omega = -0.3$. As we can see the amplitude of this wave is very large compared to the depth of the channel and its crest is sharp.
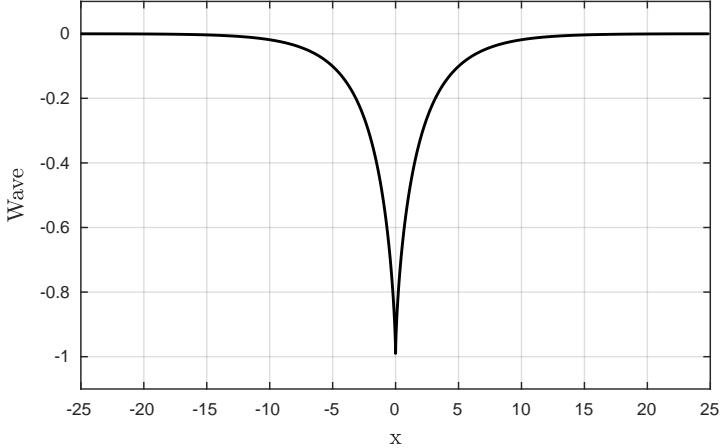
Figure 3: Steady solution for $F = 1.2$ and $\Omega = -0.3$.
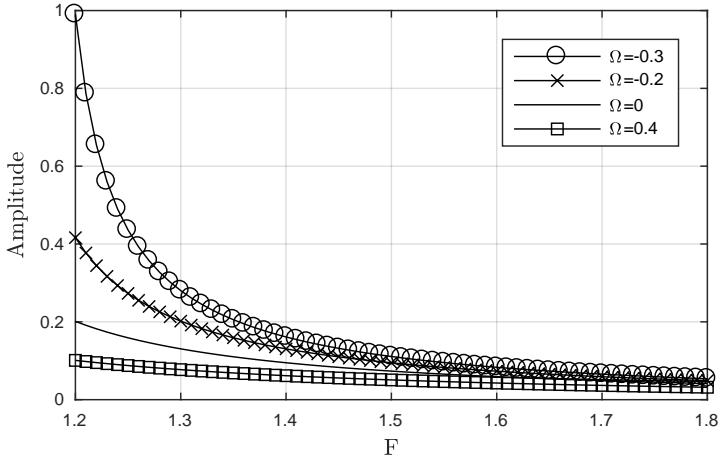
Figure 4: Amplitude of the steady waves as a function of the Froude number for different values of Ω.

In Figure 4 we see how the amplitude of the steady wave varies with the Froude number for different values of Ω. For a fixed value of Ω the amplitude decays with the Froude number. Negative values of Ω tend to sharpen the steady waves, while positive values to smoothen them. Therefore, a non-uniform current affects the amplitude as well as the regularity of the steady wave.

In the next subsection, we let the parameter ε varies and analyse the consequences on the computed steady waves.

4.2   Beyond the weakly nonlinear regime

For a shallow water channel, in the weakly nonlinear, weakly dispersive regime the fKdV model is used to study near-resonant disturbances moving along the free surface with small amplitudes. Studying steady solution for the fKdV, Binder et al. [3] showed that there is an interval $(1-R, 1)$ in which there are no steady solutions for negative forcings. Besides, the ratio using the length scales of our adimensionalization R is given as

$$R = \left(\frac{9\varepsilon^3}{4\sqrt{2}}\right)^{2/3},$$

so, it depends on the intensity of the applied pressure. Flamarion et al. [7] showed that there is a critical curve on the plane (Ω, F) in which the flow behaves like the near-resonant flow in the absence of vorticity. The curve is described as

$$F_\Omega = -\frac{\Omega}{2} + \frac{\sqrt{\Omega^2 + 4}}{2}, \tag{4.1}$$

and depicted in Figure 5.
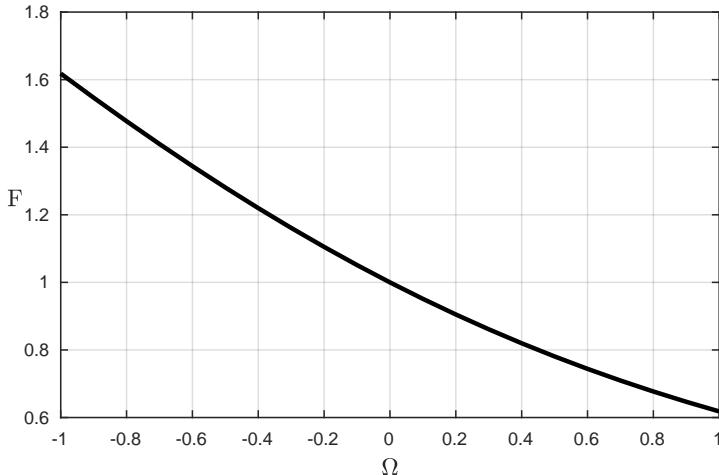
Figure 5: Critical curve on the plane $\Omega \times F$.

In this section we increase ε and see how this critical curve turns into a two-dimensional region. In this region we do not expect to find physical steady solutions. We consider a neighbourhood bellow the critical curve defined in (4.1). We find that the larger ε is, the larger is the ratio in which the numerical method does not capture physical steady waves. Numerical evidences indicate that one cannot find steady physical solutions in the region in a vicinity below the critical curve.

It is worth pointing out that the region is not uniform, however there is a uniform band where only non-physical solutions are found, and its thickness varies with ε. Table 1 shows the ratio and ε are related in the full nonlinear model and in the weakly nonlinear model. When $\varepsilon \to 0$ the ratios agree very well. Once we increase ε, they no longer agree, which is natural since the models agree only when $\varepsilon \approx 0$. It is important to notice that, the ratio of the nonlinear model is always greater than the weakly nonlinear model.

Table 1: The ratios of the nonlinear and weakly nonlinear models.

ε	Nonlinear ratio	Weakly Nonlinear ratio
0.01	0.003	0.000
0.25	0.005	0.001
0.05	0.016	0.005
0.10	0.051	0.022
0.20	0.1228	0.087
0.25	0.152	0.135

5   CONCLUSION

In this paper, we have studied steady rotational waves in a low-pressure region. Using the conformal mapping technique we constructed a numerical method to compute steady wave solutions for the Euler equations. We showed that the sheared current affects the steady solutions qualitatively as well as quantitativity. Besides, we found numerical evidences that steady waves may not exist in a bounded region of the plane $\Omega \times F$.

Acknowledgments

REFERENCES

[1] T.R. Akylas. On the excitation of long nonlinear water waves by a moving pressure distributions. *J Fluid Mech*, **141** (1984), 455–466.

[2] P. Baines. "Topographic effects in stratified flows". Cambridge University Press (1995).

[3] B.J. Binder, M. Blyth & S. Balasuriya. Non-uniqueness of steady free-surface flow at critical Froude number. *EPL (Europhysics Letters)*, **105**(4) (2014), 44003.

[4] J. Boyd. Weakly non-local solitons for capillary-gravity waves: Fifth-degree Korteweg-de Vries equation. *Physica D*, **48**(1) (1991), 129–146.

[5] W. Choi. Nonlinear surface waves interacting with a linear shear current. *Math Comput Simul*, **80** (2009), 29–36.

[6] A.L. Dyachenko, V.E. Zakharov & E.A. Kuznetsov. Nonlinear dynamics of the free surface of an ideal fluid. *Plasma Phys*, **22** (1996), 916–928.

[7] M.V. Flamarion, P.A. Milewski & A. Nachbin. Rotational waves generated by current-topography interaction. *Stud Appl Math*, **142** (2019), 433–464.

[8] M. Fracius, H.C. Hsu, C. Kharif & P. Montalvo. Gravity-capillary waves in finite depth on flows of constant vorticity. *Proc R Soc Lond A*, **472**(20160363) (2016).

[9] T. Gao, Z. Wang & P.A. Milewski. Nonlinear hydroelastic waves on a linear shear current at finite depth. *J Fluid Mech*, **876** (2019), 55–86.

[10] R. Grimshaw & M. Maleewong. Stability of steady gravity waves generated by a moving localized pressure disturbance in water of finite depth. *Phys Fluids*, **25** (2013).

[11] R. Grimshaw & M. Maleewong. Transcritical flow over two obstacles: forced Korteweg-de Vries framework. *J Fluid Mech*, **809** (2016), 918–940.

[12] R. Grimshaw & M. Maleewong. Transcritical flow over obstacles and holes: forced Korteweg-de Vries framework. *J Fluid Mech*, **881** (2019), 660–678.

[13] R. Grimshaw & N. Smyth. Resonant flow of a stratified fluid over topography in water of finite depth. *J Fluid Mech*, **169** (1986), 429–464.

[14] R.S. Johnson. Models for the formation of a critical layer in water wave propagation. *Phil Trans R Soc A*, **370** (2012), 1638–1660.

[15] A. Joseph. "Investigating Seaflaws in the Oceans". New York: Elsevier (2016).

[16] P.A. Milewski. The Forced Korteweg-de Vries Equation as a Model for Waves Generated by Topography. *CUBO A Math J*, **6**(4) (2004), 33–51.

[17] M. Peyrard. "Nonlinear excitations in biomolecules". Berlim: Springer (1994).

[18] L.J. Pratt. On nonlinear flow with multiple obstructions. *J Atmos Sci*, **41** (1984), 1214–1225.

[19] L.N. Trefethen. "Spectral Methods in MATLAB". Philadelphia: SIAM (2001).

[20] D.M. Wu & T.Y. Wu. Three-dimensional nonlinear long waves due to moving surface pressure. In: Proc 14th Symp on Naval Hydrodynamics. *Nat Acad Sci, Washington, DC*, **41** (1982), 103–125.

[21] T.Y. Wu. Generation of upstream advancing solitons by moving disturbances. *J Fluid Mech*, **184** (1987), 75–99.